Journal of Inorganic Biochemistry 206 (2020) 111016

Contents lists available at ScienceDirect

Journal of Inorganic Biochemistry

journal homepage: www.elsevier.com/locate/jinorgbio

Silver nanoparticle synthesis in human ferritin by photochemical reduction

Italo Moglia[a,b,1], Margarita Santiago[a,b,1], Monica Soler[a], Alvaro Olivera-Nappa[a,b,*]

[a] Department of Chemical Engineering, Biotechnology and Materials, FCFM, University of Chile, Beauchef 851, Santiago, Chile
[b] Center for Biotechnology and Bioengineering – CeBiB, FCFM, University of Chile, Beauchef 851, Santiago, Chile

ARTICLE INFO

Keywords:
Ferritin
Silver nanoparticles
Chemical reduction
Photochemical reduction

ABSTRACT

Ferritin is a globular hollow protein that acts as the major iron storage protein across living organisms. The 8 nm-diameter internal cavity of ferritin has been used as a nanoreactor for the synthesis of various metallic nanoparticles different to iron oxides. For this purpose, ferritin is incubated in solution with metallic ions that enter the cavity through its natural channels. Then, these ions are subjected to a reduction step to obtain highly monodisperse metallic nanoparticles, with enhanced stability and biocompatibility provided by the ferritin structure. Potential biomedical applications of ferritin-nanoparticle complex will require the use of human ferritin to provide a safer and low-risk alternative for the delivery of metallic nanoparticles into the body. However, most of the reported protocols for metallic nanoparticles synthesis uses horse spleen ferritin as nanocontainer. Previous studies have acknowledged technical difficulties with recombinant human ferritin during the synthesis of metallic nanoparticles, like protein precipitation, which is translated into low recovery yields. In this study, we tested a novel photochemical reduction method for silver nanoparticle synthesis in human recombinant ferritin and compared it with the traditional chemical reduction method. The results show that photoreduction of silver ions inside ferritin cavity provides a universal method for silver nanoparticle synthesis in both recombinant human ferritin homopolymers (Light and Heavy ferritin). Additionally, we report important parameters that account for the efficiency of the method, such as ferritin recovery yield (~60%) and ferritin-silver nanoparticle yield (34% for H-ferritin and 17% for L-ferritin).

1. Introduction

Ferritin is the major iron storage protein ubiquitous among living organisms. Maxiferritins, the variety present in vertebrates, are assembled from 24 subunits that form a hollow spherical shell with an inner and outer diameter of ~8 and ~12 nm, respectively [1]. Vertebrate ferritins are heteropolymers formed by two homologous subunits, the H (heavy) and the L (light) chains, which vary in proportions depending on its origin [2]. Each subunit type has a particular role within the structure. The H chain contains a ferroxidase active center [3–5] that catalyzes the oxidation of Fe^{+2} into Fe^{+3} with O_2, and L chains contain sites for the nucleation of iron oxyhydroxide crystals [6]. Ferritin structure has eight 3-fold symmetry channels that provide the pathway for Fe^{+2} flux from the outer environment into the inner cavity that are subsequently oxidized and mineralized inside the internal cavity, facilitated by the presence of negative electric charge amino acidic residues [7,8].

Ferritin has been used technologically as a nanocontainer for non-biological metallic nanoparticle synthesis, because its cavity offers a constrained space to obtain monodisperse particles and its structure also contribute to improve nanoparticle stability [9,10]. Different ferritin templates, especially horse spleen ferritin, have been used as a nanoreactor to synthesize a variety of metallic nanoparticles in its cavity, such as Mn, Co, Ni, Pd, Pt, Ag, Au [11,12]. There is a special interest in metallic nanoparticles for detection and therapeutic applications in biomedicine, for example ferritin containing supermagnetic iron oxides (Fe_3O_4) for Magnetic Resonance Imaging [13], Au-containing ferritin as biosensor for detecting single-nucleotide polymorphisms [14] and Ag-containing ferritin for inducing cell death [15].

Biomedical utilization of recombinant human ferritin containing a metallic nanoparticle requires the standardization and improvement of protocols for nanoparticle synthesis. Based on experimental evidence, a human ferritin nanocontainer for intracellular delivery should contain H-chain subunits, because these subunit-types mediate cellular uptake through interaction with the transferrin receptor [16]. Recombinant human H ferritin homopolymers have been shown to be successfully internalized by different cell types, like macrophages [17], tumor cells [15,18–21]. Also, in murine models, human H ferritin homopolymers

* Corresponding author at: Department of Chemical Engineering, Biotechnology and Materials, FCFM, University of Chile, Beauchef 851, Santiago, Chile.
E-mail address: aolivera@ing.uchile.cl (A. Olivera-Nappa).
[1] These authors contributed equally to this study.

https://doi.org/10.1016/j.jinorgbio.2020.111016
Received 18 October 2019; Received in revised form 28 January 2020; Accepted 30 January 2020
Available online 01 February 2020
0162-0134/

have been targeted to gliomas [22], lymph nodes [23], murine carotid and abdominal aortic aneurysm disease [24,25], and tumors [13,20,21,26–29]. Contrarily, a ferritin-based nanocontainer for an extracellular biomedical application, e.g. a topical skin product, should be only composed of L-chain subunits to avoid cellular internalization.

The synthesis of noble metal nanoparticles inside human ferritin has not been exempt of difficulties. Recombinant human L and H ferritins are prone to precipitate during silver nanoparticle synthesis when compared to the resistant *Pyrococcus furiosus* ferritin, in which silver nanoparticles were successfully synthesized [12]. However, using controlled conditions such as a low concentration of H human ferritin (0.1 mg/mL), which consequently requires a reduced amount of Ag ions (ferritin/Ag ratio of 1:100–1:2000) and addition of a limited amount of reducing agent (ferritin/$NaBH_4$ ratio of 1:250) allowed the formation of silver nanostructures [30]. Other strategies had been the chemical or genetic modification of human ferritin to create a compatible container for noble metal nanoparticle synthesis. The blockage or removal of cysteines from the exterior surface of H-chain ferritin and the incorporation of cysteines on the interior surface allowed gold and silver nanoparticle synthesis [15,31]. Also, the fusion of a dodecapeptide able to reduce silver ions into the C-terminal of human L-chain, which locates into the cavity, has been shown to produce Ag nanoparticles with 60% efficiency [32].

In this study, we used two methods to synthesize silver nanoparticles inside recombinant human ferritin, using a chemical and a novel photochemical agent to reduce the silver cations inside ferritin cavity. Our results demonstrate that the photochemical method is superior than the chemical one and allows the synthesis of silver nanoparticles in human L and H homopolymeric ferritin preserving the structural integrity and colloidal stability of the protein nanocage.

2. Experimental

2.1. L and H-ferritin expression and purification

cDNA from colorectal adenocarcinoma (Caco-2) cells, donated by Dr. M. Tulio Nuñez, was used for amplification of L and H ferritin genes. Primers were designed based on the sequences available in Genbank (NM_002032.2 and NM_000146.3) introducing restriction endonuclease cleavage sites for cloning the fragments into pET28a digested with *Nde*I and *Xho*I. The final plasmids pET-FTL and pET-FTH were verified by DNA sequencing.

The plasmids were transformed into *E. coli* BL21 DE3 and protein expression was induced by growing the cells in autoinduction media for 20 h at 25 °C with shaking at 250 RPM. Cells were harvested at 6000*g* for 10 min, resuspended in 50 mM Tris pH 8 and disrupted by sonication. The cell extracts were heated at 75 °C for 10 min and clarified. Then the ferritin extracts were purified through a Q-sepharose column eluting with a linear gradient (0–1 M) of NaCl using an ÄKTA Avant system (GE Healthcare Life Sciences). The fractions containing ferritin were concentrated and finally purified using a Superdex 200 Increase 10/300 GL column, recovering the monomeric ferritin fraction. All expression and purification steps were performed using iron-free media and solutions to ensure the obtention of apoferritin.

2.2. Ag nanoparticle synthesis

A 1 mL of 2 mg/mL ferritin (Ft) solution in 50 mM Tris pH 8 with the addition of 44.4 μL of a 100 mM solution of $AgNO_3$ (equivalent to 1000 Ag atoms per ferritin molecule, 1000 Ag/Ft) was incubated overnight at 4 °C. Next day, the excess of metallic ions were removed by dialysis against 50 mM Tris pH 8. Chemical reduction was performed by adding 44.4 μL of a 100 mM solution of $NaBH_4$. Alternatively, photoreduction was achieved by addition of 89 μL of a 50 mM solution of Irgacure 2959 photoreducer (2-Hydroxy-4′-(2-hydroxyethoxy)-2-methyl-propiophenone, Sigma 410896), incubated 1 h at 4 °C, then exposed to UV-A light (320–400 nm, 64 W) for 20 to 30 min at room temperature. After chemical reduction and photoreduction were performed, the samples were centrifuged at 14,000 rpm for 10 min at 4 °C, then the soluble fraction was dialyzed against 50 mM Tris pH 8 and stored at 4 °C. Nanoparticle synthesis in ferritin was performed in duplicate.

2.3. Characterization techniques

Protein quantification was carried out using the modified Lowry method (Thermo Fisher Scientific #23240) with Bovine Serum Albumin (BSA) as a reference. Optical properties of the protein samples with nanoparticles were measured using UV–vis spectroscopy with an AvaSpec-2048 (Avantes). Ferritin samples containing silver nanoparticles were subjected to size exclusion chromatography (SEC) using a FPLC ÄKTA Avant using a Superdex 200 Increase 10/300 GL column, measuring absorbance at 280 and 410 nm for protein and silver plasmon detection, respectively. Ferritin protein samples were analyzed in native 6% polyacrylamide electrophoresis gels (PAGE). Transmission Electron Microscopy (TEM) characterization was performed using a Philips Tecnai 12 equipment operated at 80 kV in the Advanced Microscopy Facility, at the Pontificia Universidad Católica de Chile. The statistical analysis of size distribution of ferritin protein shells and silver nanoparticles was performed using ImageJ software by sampling over 100 particles.

3. Results and discussion

3.1. Synthesis of silver nanoparticle in L and H human ferritin

The synthesis of silver nanoparticles (Ag-NP) in recombinant L-chain (FTL) or H-chain (FTH) human ferritin was performed controlling every step to avoid precipitation. For this, an overnight incubation at 4 °C of the ferritin solution with silver ions (molar ratio 1000 Ag/Ft) was performed to ensure ferritin loading. Then, excess silver ions were removed from the solution by dialysis, followed by reduction of the Ag ions inside the cavity to produce Ag^0. Two different reducing methods were tested, chemical reduction and photochemical reduction (Fig. 1). The chemical method consisted in the addition of $NaBH_4$ (1 equivalent per Ag atom), which is the most reported reducing agent used in the synthesis of metallic nanoparticles in ferritin [12,30,33,34]. In the photochemical reduction method, the photoinitiator I-2959 was added to the ferritin sample (1 equivalent per Ag atom) and incubated under UV-A light. This method is proposed as a milder alternative to $NaBH_4$ and has been proven to work for silver nanoparticles stabilized by citrate and albumin [35–37].

The addition of the silver salt ($AgNO_3$) produces slight turbidity in FTL and FTH solutions, which did not increase during overnight incubation. The turbidity was retained after dialysis, but samples remained soluble. The reducing step caused the appearance of color in FTL samples, which was stronger in the sample reduced with I-2959 compared to $NaBH_4$. Both samples remained coloured after the centrifugation step used to remove precipitates or aggregates (Fig. 2A). On the other hand, only reduction by I-2959 in FTH produced color that remained soluble after the centrifugation step. Contrarily, the addition of $NaBH_4$ to FTH induced bulk coloured precipitation, leaving a translucent non-coloured solution after the centrifugation step (Fig. 2B).

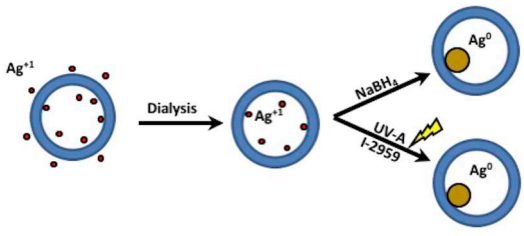

Fig. 1. Diagram of Ag-nanoparticle synthesis in human apoferritin cavity.

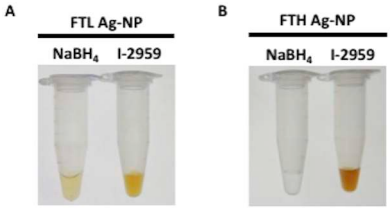

Fig. 2. Synthesis of silver nanoparticles in L and H human ferritin. Soluble fraction of the L-chain ferritin (A) and H-chain (B) ferritin samples color after the Ag-NP synthesis process using two reduction methods ($NaBH_4$ or I-2959).

Table 1
Protein recovery yield after Ag-NP synthesis.

Sample	FTL Ag-NP		FTH Ag-NP	
	$NaBH_4$	I-2959	$NaBH_4$	I-2959
Protein recovery	55%	60%	~0%	63%

The protein content in the soluble fraction of the samples was quantified after Ag-NP synthesis to calculate the protein recovery yield. The results show that FTL-Ag-NP samples have a protein recovery yield of 55–60%, independently of the reduction method for nanoparticle synthesis (Table 1). A similar value (63%) was obtained for FTH-Ag-NP produced by photoreduction. As expected, the protein recovery of the FTH-Ag-NP sample produced by chemical reduction was under the limit of detection, confirming the negative effect caused by $NaBH_4$ addition on FTH structure and colloidal stability.

This massive precipitation of FTH during silver reduction with $NaBH_4$ can be explained by the differences in ferritin properties and reduction kinetics. FTH and FTL subunit types have a very high structural homology that allows the formation of a hetero 24-mer cage, but also possess important functional differences. It is known, for instance, that FTH structure is more sensitive to acidic denaturation than the FTL homopolymer due to the lack of a salt-bridge [38]. These structural differences could also have an effect on FTH stability under strong reducing conditions exerted by $NaBH_4$. In addition, the FTH homopolymer has multiple ion chelation centers and a strong negative inner electrostatic potential that allow specific interactions with various cations, including Ag+ [12,30,39]. Thus, having more silver ions attached to the FTH structure, added to the fast reduction exerted by $NaBH_4$, could favor the formation of many small silver clusters that somehow destabilize the tertiary protein structure. On the contrary, the FTH structure is not affected by photoreduction of silver ions, possibly explained by the slower kinetics or the differences in silver nanoparticle growth in this process.

Interestingly, the FTL homopolymer structure resisted the silver $NaBH_4$ reduction process, opposite to the results reported by Kasyutich et al. [12], where massive precipitation occurred for H and L homopolymers, suggesting that other experimental conditions (such as protein concentration, buffers, pH or others) could be playing an important role in protein stability during reduction.

3.2. Characterization of ferritin containing Ag nanoparticles

The optical absorbance properties of the ferritin Ag-NP samples were analyzed by UV–visible spectrophotometry in the range of 180 to 800 nm to evaluate the formation of Ag-NP by the detection of the surface resonance plasmon (SRP) absorbance peak. The spectra for FTL Ag-NP samples show the SRP at 404 nm for both reduction methods (Fig. 3A), suggesting a similar nanoparticle size formed in FTL cavity despite the reducing agent used. From this, we can deduce that reduction rate does not affect the final size of the metallic core, suggesting that nanoparticle synthesis in the FTL is limited by the amount of Ag^+

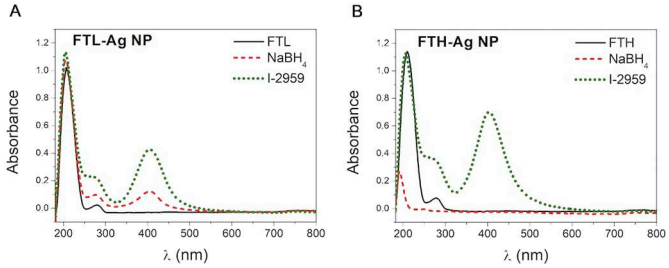

Fig. 3. UV–visible spectrum of silver nanoparticles in L and H human ferritin. L-chain ferritin (A) and H-chain (B) ferritin samples UV–vis spectra after Ag-NP synthesis process using two reductions methods ($NaBH_4$ or I-2959). The spectra of the control samples (FTL and FTH) show the absorption of ferritin subjected to the same reduction methods without the addition of silver ions.

incorporated in the inner cavity. The observed difference in the absorbance intensity of SRP between FTL Ag-NP produced by the two different reducing method can be attributed to a higher content of Ag-NP in the oligomeric fraction obtained by photoreduction compared to the chemical method. Also, these samples exhibit ferritin characteristic absorption peaks at 280 nm and 204 nm, attributed to aromatic amino acids and peptide bonds respectively, indicating conservation of the protein primary structure.

The spectra of the FTH Ag-NP sample subjected to photoreduction showed SRP peaks at 402 nm and protein characteristic absorption peaks at 280 and 205 nm. The SRP in FTH showed a very slight blue shift (~2 nm) compared to FTL Ag-NP which may indicate a smaller average size of the metallic core. This could be explained by the highest synthesis efficiency observed in FTH compared to FTL, resulting in less Ag atoms available per ferritin to increase the nanoparticle size. The spectra of FTH Ag-NP (Fig. 3B) obtained by chemical reduction did not show SRP absorption peaks and exhibited low absorbance of the protein peaks, which was expected after the precipitation observed during nanoparticle synthesis and confirmed by the low protein recovery yield (Table 1).

Independently of the ferritin homopolymer and reduction method, all UV–Vis spectra of ferritin nanocages with Ag-NP inside exhibit an increment of the absorbance at 280 nm compared with empty ferritin. This effect can be attributed to the light absorption and dispersion exerted by the Ag nanoparticles [40,41]. A similar phenomenon was observed in a previous work of our group where horse spleen ferritin shows an increased absorption at 280 nm that is related in a nonlinear way to the iron oxide content of the ferritin nanocages [42].

Additionally, the presence of silver clusters with less than 2 nm in diameter inside ferritin was studied by fluorescence measurements (λ_{exc} 470 nm/λ_{emm} 695 nm; according to Lee et al. [30]). All the ferritin-Ag-NP samples showed no fluorescence (data not shown), which rules out the presence of fluorescent silver nano-clusters smaller than 2 nm.

Ferritin Ag-NP samples were characterized by SEC and native polyacrylamide electrophoresis PAGE to evaluate the structural integrity of the protein-NP complex. The protein and Ag-NP were detected by following the absorbance at 280 nm and 410 nm, respectively (as in Fig. 3). The chromatograms show two protein elution peaks at 280 nm (A_{280nm}), demonstrating the existence of two different species in each sample, previously reported by our group and other authors [42–44]. The first protein elution peak at 8.4 mL (void volume) corresponds to ferritin aggregated species like dimers, trimers or higher oligomers, while the second elution peak at 10.4 mL corresponds to monomeric ferritin nanocages. The chromatograms of the FTL-Ag-NP samples (Fig. 4A) show the coelution of the Ag-NP absorbance peak at 410 nm (A_{410nm}) with the first protein elution peak at 8.4 mL, which corresponds to oligomeric protein species. The same elution profile was observed in the chromatogram of the FTH-Ag-NP sample synthesized with I-2959 (Fig. 4B, lower panel). As expected, almost no detectable absorbance peak at 410 nm was observed for the sample FTH-Ag-NP synthetized with $NaBH_4$ (Fig. 4B, upper panel). These results indicate

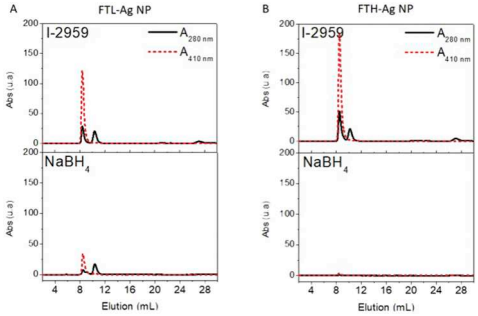

Fig. 4. Size exclusion chromatograms of the samples FTL and FTH with Ag-NP. (A) FTL samples reduced with $NaBH_4$ or I-2959. (B) FTH samples reduced with $NaBH_4$ or I-2959. Chromatograms of the samples reduced with I-2959 show a small elution peak at 27 mL that correspond to remnants of the photoinitiator that persisted after dialysis.

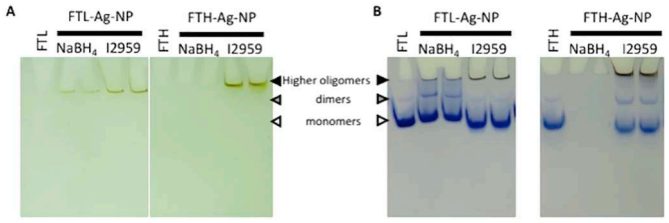

Fig. 5. Native polyacrylamide gel for Ferritin Ag-NP samples. (A) Gel before Coomassie staining for nanoparticle detection. (B) Gel after Coomassie staining for protein detection. FTL and FTH are control samples without Ag-NP. Ferritin-Ag-NP samples were run in duplicate.

that Ag-NP and ferritin oligomers are associated, which suggests that ferritin monomers do not contain Ag nanoparticles because of the lack of absorption at 410 nm. This was also demonstrated from native polyacrylamide gel electrophoresis, where Ag nanoparticles are associated to higher oligomers of H and L ferritin that slightly penetrated the gel and got concentrated at the bottom of the sample well (Fig. 5). Contrarily, the ferritin-Ag-NP monomeric and dimeric bands show not detectable color from the nanoparticles. Considering that the starting material was purified monomeric ferritin, these oligomeric species are formed during the synthesis process, either during silver cation loading and/or silver reduction.

Silver cations have been proven to induce changes in the secondary structure of other proteins such as BSA [45]. Potentially, the incorporation of Ag ions onto ferritin could trigger some local conformational or chemical changes of amino acids of the peptidic structure, which could lead to a new distribution of electrical charges on the surface, decreasing the electrostatic repulsion of the protein and therefore favoring the formation of oligomers, leaving ferritin molecules without silver content as monomers. This effect has also been observed for iron oxide-containing ferritin, in which the amount of oligomeric forms was reduced after iron removal [42].

The efficiency of NP formation in ferritin, corresponding to the fraction of the recovered protein associated with silver nanoparticles, was calculated for photoreduced samples after SEC fractioning by dividing protein concentration in the fraction containing Ag-NP (oligomeric fraction) by the total protein concentration (monomeric and oligomeric fraction). FTH showed a higher NP formation efficiency (54%), compared to 28% for FTL, suggesting that the process of silver incorporation and nanoparticle synthesis is not homogenous and strongly depends on the type of homopolymer used.

All ferritin-Ag-NP samples were observed by TEM to check the structural integrity of the protein and measure nanoparticle size distributions. Negative uranyl acetate staining was used for protein shell visualization (Fig. 6A). Silver nanoparticles were directly observed with no staining (Fig. 6B). The images with negative staining show the spherical protein cage with an external diameter close to 12 nm for all samples, indicating that the nanoparticle synthesis process did not affect the overall protein structure. Images obtained without staining allowed the observation of electron-dense spherical metallic cores. The mean diameter of the observed nanoparticles were 5.4 ± 2 nm and 5.3 ± 2.3 nm for FTL-Ag-NP obtained by chemical and photoreduction methods, respectively. Nanoparticles synthesized in FTH by photoreduction show a mean diameter of 3.2 ± 1.5 nm, which is smaller than the Ag-NP in FTL, in accordance with the SRP slight blue shift observed for this sample (Fig. 3B).

In all cases, silver nanoparticles were smaller than the ferritin internal diameter, strongly suggesting that the cavity of FTH and FTL apoferritin is acting as a size-constraining reactor for nanoparticle synthesis.

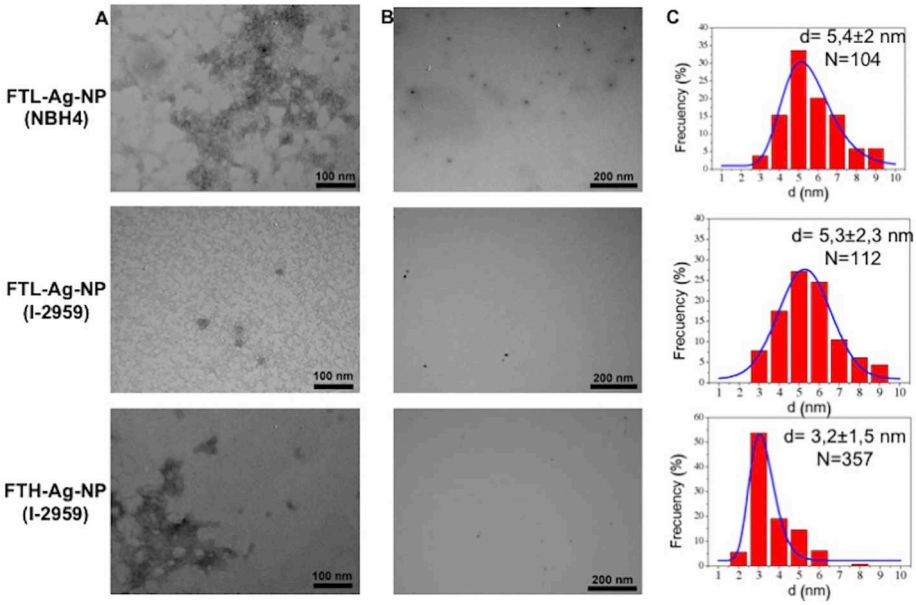

Fig. 6. TEM images of ferritin-Ag-NP samples. (A) Ferritin-Ag-NP samples negatively stained with uranyl acetate. (B) Ferritin-Ag-NP samples observed without stain. (C) Size distributions of the silver nanoparticles.

4. Conclusions

We compared two different reduction methods for the synthesis of Ag-NP inside two ferritin nanocontainers: recombinant human ferritin H homopolymer (FTH) and recombinant human ferritin L homopolymer (FTL). The chemical method was not suitable to obtain Ag-NP inside FTH nanocages because it has a detrimental effect on protein structural integrity and colloidal stability. On the other hand, FTL, which is a structural homologous of FTH, was not especially affected by the chemical reduction method for silver nanoparticle synthesis with a protein recovery yield of 55%. The photochemical reduction method allows the synthesis of silver nanoparticles in both ferritins with ~60% protein recovery. Also, this method showed a higher efficiency of synthesis for silver nanoparticle in FTH than in FTL. Electron microscopy size determination of Ag-NP inside ferritin cavities, showed that silver nanoparticles were smaller in FTH (3 nm) compared to those synthesized inside FTL (5 nm) under our experimental conditions. Finally, we also show that Ag-NP synthesis in ferritin induces the oligomerization of the nanocages containing the metallic nanoparticle. In conclusion, we herein presented a novel universal method for silver nanoparticle synthesis inside recombinant human ferritin – based on photoreduction – that is suitable for biomedical applications, preserves ferritin structure, gives a high protein recovery yield and significantly increases nanoparticle formation efficiency over previous methods.

Abbreviations

Ft	ferritin
FTL	L-ferritin
FTH	H-ferritin
Ag-NP	silver nanoparticle
FTL-Ag-NP	L-ferritin containing silver nanoparticle
FTH-Ag-NP	H-ferritin containing silver nanoparticle
BSA	Bovine Serum Albumin
SEC	size exclusion chromatography
PAGE	polyacrylamide gel electrophoresis
I-2959	Irgacure 2959
SRP	surface resonance plasmon
TEM	Transmission Electron Microscopy

Declaration of competing interest

The authors declare that they have no known competing financial interests or personal relationships that could have appeared to influence the work reported in this paper.

Acknowledgment

The authors would like to thank Dr. M. Tulio Núñez for providing Caco-2 cell cDNA and Alejandro Munizaga from the Advanced Microscopy Facility at the Pontificia Universidad Católica de Chile for his support for TEM microphotograph acquisition. The authors would also like to acknowledge CONICYT funding for the acquisition of the ÄKTA Avant purification system used in this study (Fondequip EQM160019 project) and for funding provided by the Centre for Biotechnology and Bioengineering – CeBiB (PIA FB0001 project).

References

[1] Z. Wang, H. Gao, Y. Zhang, G. Liu, G. Niu, X. Chen, Front. Chem. Sci. Eng. 11 (2017) 633–646.
[2] L. Zhang, M. Knez, J. Nanosci. Lett. (2012) 2.
[3] F. Bou-Abdallah, G. Zhao, G. Biasiotto, M. Poli, P. Arosio, N.D. Chasteen, J. Am. Chem. Soc. 130 (2008) 17801–17811.
[4] D.E. Bacelo, R. Binning Jr., Chem. Phys. Lett. 507 (2011) 174–177.
[5] D.M. Lawson, A. Treffry, P.J. Artymiuk, P.M. Harrison, S.J. Yewdall, A. Luzzago, G. Cesareni, S. Levi, P. Arosio, FEBS Lett. 254 (1989) 207–210.
[6] C. Pozzi, S. Ciambellotti, C. Bernacchioni, F. Di Pisa, S. Mangani, P. Turano, Proc. Natl. Acad. Sci. 114 (2017) 2580–2585.
[7] T. Takahashi, S. Kuyucak, Biophys. J. 84 (2003) 2256–2263.
[8] R.K. Behera, E.C. Theil, Proc. Natl. Acad. Sci. U. S. A. 111 (2014) 7925–7930.
[9] B. Bhushan, S.U. Kumar, I. Matai, A. Sachdev, P. Dubey, P. Gopinath, J. Biomed. Nanotechnol. 10 (2014) 2950–2976.
[10] G. Jutz, P. van Rijn, B. Santos Miranda, A. Boker, Chem. Rev. 115 (2015) 1653–1701.
[11] H. Yoshimura, Colloids Surf. A Physicochem. Eng. Asp. 282 (2006) 464–470.
[12] O. Kasyutich, A. Ilari, A. Fiorillo, D. Tatchev, A. Hoell, P. Ceci, J. Am. Chem. Soc. 132 (2010) 3621–3627.
[13] K. Fan, C. Cao, Y. Pan, D. Lu, D. Yang, J. Feng, L. Song, M. Liang, X. Yan, Nat. Nanotechnol. 7 (2012) 459–464.
[14] F. Yu, G. Li, B. Qu, W. Cao, Biosens. Bioelectron. 26 (2010) 1114–1117.
[15] L. Mosca, E. Falvo, P. Ceci, E. Poser, I. Genovese, G. Guarguaglini, G. Colotti, Appl. Sci. 7 (2017) 101.
[16] L. Li, C.J. Fang, J.C. Ryan, E.C. Niemi, J.A. Lebron, P.J. Bjorkman, H. Arase, F.M. Torti, S.V. Torti, M.C. Nakamura, W.E. Seaman, Proc. Natl. Acad. Sci. U. S. A. 107 (2010) 3505–3510.
[17] M. Uchida, M. Terashima, C.H. Cunningham, Y. Suzuki, D.A. Willits, A.F. Willis, P.C. Yang, P.S. Tsao, M.V. McConnell, M.J. Young, Magn. Reson. Med. 60 (2008) 1073–1081.
[18] M. Uchida, M.L. Flenniken, M. Allen, D.A. Willits, B.E. Crowley, S. Brumfield, A.D. Willis, L. Jackiw, M. Jutila, M.J. Young, T. Douglas, J. Am. Chem. Soc. 128 (2006) 16626–16633.
[19] K. Li, Z.-P. Zhang, M. Luo, X. Yu, Y. Han, H.-P. Wei, Z.-Q. Cui, X.-E. Zhang, Nanoscale 4 (2012) 188–193.
[20] Z. Zhen, W. Tang, H. Chen, X. Lin, T. Todd, G. Wang, T. Cowger, X. Chen, J. Xie, ACS Nano 7 (2013) 4830–4837.
[21] Z. Zhen, W. Tang, C. Guo, H. Chen, X. Lin, G. Liu, B. Fei, X. Chen, B. Xu, J. Xie, ACS Nano 7 (2013) 6988–6996.
[22] K. Fan, X. Jia, M. Zhou, K. Wang, J. Conde, J. He, J. Tian, X. Yan, ACS Nano 12 (2018) 4105–4115.
[23] B.-R. Lee, H.K. Ko, J.H. Ryu, K.Y. Ahn, Y.-H. Lee, S.J. Oh, J.H. Na, T.W. Kim, Y. Byun, I.C. Kwon, K. Kim, J. Lee, Sci. Rep. 6 (2016) 35182.
[24] T. Kitagawa, H. Kosuge, M. Uchida, M.M. Dua, Y. Iida, R.L. Dalman, T. Douglas, M.V. McConnell, Mol. Imaging Biol. 14 (2012) 315–324.
[25] T. Kitagawa, H. Kosuge, M. Uchida, Y. Iida, R.L. Dalman, T. Douglas, M.V. McConnell, J. Magn. Reson. Imaging 45 (2017) 1144–1153.
[26] M. Liang, K. Fan, M. Zhou, D. Duan, J. Zheng, D. Yang, J. Feng, X. Yan, Proc. Natl. Acad. Sci. 111 (2014) 14900–14905.
[27] X. Lin, J. Xie, G. Niu, F. Zhang, H. Gao, M. Yang, Q. Quan, M.A. Aronova, G. Zhang, S. Lee, R. Leapman, X. Chen, Nano Lett. 11 (2011) 814–819.
[28] X. Lin, J. Xie, L. Zhu, S. Lee, G. Niu, Y. Ma, K. Kim, X. Chen, Angew. Chem. Int. Ed. 50 (2011) 1569–1572.
[29] X. Li, L. Qiu, P. Zhu, X. Tao, T. Imanaka, J. Zhao, Y. Huang, Y. Tu, X. Cao, Small 8 (2012) 2505–2514.
[30] I.H. Lee, B. Ahn, J.M. Lee, C.S. Lee, Y. Jung, Analyst. 140 (2015) 3543–3550.
[31] C.A. Butts, J. Swift, S.G. Kang, L. Di Costanzo, D.W. Christianson, J.G. Saven, I.J. Dmochowski, Biochemistry 47 (2008) 12729–12739.
[32] R.M. Kramer, C. Li, D.C. Carter, M.O. Stone, R.R. Naik, J. Am. Chem. Soc. 126 (2004) 13282–13286.
[33] J.M. Domínguez-Vera, N. Gálvez, P. Sánchez, A.J. Mota, S. Trasobares, J.C. Hernández, J.J. Calvino, Eur. J. Inorg. Chem. 2007 (2007) 4823–4826.
[34] Y. Shin, A. Dohnalkova, Y. Lin, J. Phys. Chem. C 114 (2010) 5985–5989.
[35] K.G. Stamplecoskie, J.C. Scaiano, J. Am. Chem. Soc. 132 (2010) 1825–1827.
[36] E.I. Alarcon, C.J. Bueno-Alejo, C.W. Noel, K.G. Stamplecoskie, N.L. Pacioni, H. Poblete, J. Scaiano, J. Nanopart. Res. 15 (2013) 1374.
[37] E.I. Alarcon, M. Griffith, K.I. Udekwu, Silver Nanoparticle Applications, Springer, 2015.
[38] P. Santambrogio, S. Levi, P. Arosio, L. Palagi, G. Vecchio, D.M. Lawson, S.J. Yewdall, P.J. Artymiuk, P.M. Harrison, R. Jappelli, G. Cesareni, J. Biol. Chem. 267 (1992) 14077–14083.
[39] T. Ueno, M. Abe, K. Hirata, S. Abe, M. Suzuki, N. Shimizu, M. Yamamoto, M. Takata, Y. Watanabe, J. Am. Chem. Soc. 131 (2009) 5094–5100.
[40] K.C. Song, S.M. Lee, T.S. Park, B.S. Lee, Korean J. Chem. Eng. 26 (2009) 153–155.
[41] M. Treguer, F. Rocco, G. Lelong, A. Le Nestour, T. Cardinal, A. Maali, B. Lounis, Solid State Sci. 7 (2005) 812–818.
[42] I. Moglia, M. Santiago, A. Olivera-Nappa, M. Soler, J. Inorg. Biochem. 183 (2018) 184–190.
[43] J.D. Keyes, R.J. Hilton, J. Farrer, R.K. Watt, J. Nanopart. Res. 13 (2011) 2563–2575.
[44] O.D. Petrucci, R.J. Hilton, J.K. Farrer, R.K. Watt, J. Nanomater. (2019) 2019.
[45] X. Zhao, R. Liu, Y. Teng, X. Liu, Sci. Total Environ. 409 (2011) 892–897.